

A *Spitzer* Census of Transitional Protoplanetary Disks with AU-Scale Inner Holes

James Muzerolle^{1,2}, Lori E. Allen³, S. Thomas Megeath⁴, Jesús Hernández^{5,6} Robert A. Gutermuth⁷

ABSTRACT

Protoplanetary disks with AU-scale inner clearings, often referred to as transitional disks, provide a unique sample for understanding disk dissipation mechanisms and possible connections to planet formation. Observations of young stellar clusters with the *Spitzer* Space Telescope have amassed mid-infrared spectral energy distributions for thousands of star-disk systems from which transition disks can be identified. From a sample of 8 relatively nearby young regions ($d \lesssim 400$ pc), we have identified about 20 such objects, which we term “classical” transition disks, spanning a wide range of stellar age and mass. We employed strict infrared continuum criteria to limit ambiguity: an 8 to 24 μm spectral slope limit ($\alpha > 0$) to select for robust optically thick outer disks, and 3.6 to 5.8 μm spectral slope and 5.8 μm continuum excess limits to select for optically thin or zero continuum excess from the inner few AU of the disks. We also identified two additional categories representing more ambiguous cases: “warm excess” objects with transition-like spectral energy distributions but moderate excess at 5.8 μm , and “weak excess” objects with smaller 24 μm excess that may be optically thin or exhibit advanced dust grain growth and settling. From existing $\text{H}\alpha$ emission measurements, we find evidence for different accretion activity among the three categories, with a majority of the classical and warm excess transition objects

¹Space Telescope Science Institute, 3700 San Martin Dr., Baltimore, MD 21218

²Steward Observatory, 933 N. Cherry Ave., The University of Arizona, Tucson, AZ 85721

³National Optical Astronomy Observatory, 950 N. Cherry Ave., Tucson, AZ 85719

⁴Ritter Observatory, Department of Physics and Astronomy, University of Toledo, 2801 W. Bancroft Ave., Toledo, OH 43606

⁵Department of Astronomy, University of Michigan, 830 Dennison Building, 500 Church Street, Ann Arbor, MI 48109

⁶Centro de Investigaciones de Astronomía, Apdo. Postal 264, Mérida 5101-A, Venezuela

⁷Five Colleges Astronomy Dept., Smith College, Northampton, MA 01063

still accreting gas through their inner holes and onto the central stars, while a smaller fraction of the weak transition objects are accreting at detectable rates. We find a possible age dependence to the frequency of classical transition objects, with fractions relative to the total population of disks in a given region of a few percent at 1-2 Myr rising to 10-20% at 3-10 Myr. The trend is even stronger if the weak and warm excess objects are included. This relationship may be due to a dependence of the outer disk clearing timescale with stellar age, suggesting a variety of clearing mechanisms working at different times, or it may reflect that a smaller fraction of all disks actually undergo an inner clearing phase at younger ages. Classical transition disks appear to be less common, and weak transition disks more common, around lower-mass stars ($M \lesssim 0.3M_{\odot}$), which we suggest may be a further indicator of the stellar mass-dependent disk evolution that has been seen in previous studies. The difference in number statistics and accretion activity between the two classes further suggests that they are not connected but rather represent distinct evolutionary outcomes for disks.

Subject headings: accretion disks, stars: pre-main sequence, planetary systems: protoplanetary disks

1. Introduction

The lifetimes of circumstellar disks around young stars determine the relevant timescales available for planet formation to occur. Observational estimates are essential for constraining theories such as the core accretion (Pollack et al. 1996) and gravitational instability (Boss 1997) models. A considerable amount of work has gone into estimating disk lifetimes primarily by examining infrared excess emission as a function of age. Previous studies focused on near-infrared emission probing the innermost regions of disks have indicated typical disk lifetimes of roughly 3 Myr, with a wide dispersion from 1-10 Myr (Strom et al. 1989; Haisch et al. 2001; Hillenbrand 2005).

Constraints on the lifetime of disk material in the planet formation zone of 0.1-10 AU have been more difficult to achieve because of sensitivity and resolution limitations at the longer wavelengths which probe cooler dust. Early results from ground-based and IRAS observations of the nearby Taurus star forming region by Skrutskie et al. (1990) first identified a small population of disks “in transition”, lacking excess emission at $\lambda \lesssim 10 \mu\text{m}$ but exhibiting considerable emission at longer wavelengths and thus implying a lack of dust (at least in small grains) in the inner few AU of the disks. Given the age of Taurus, Skrutskie et al. estimated a typical transition timescale of ~ 0.3 Myr.

A handful of such transition disks with inner “holes” have been studied in some detail in recent years¹. Calvet et al. (2002) modeled the spectral energy distribution (SED) of the 10 Myr-old classical T Tauri star (CTTS) TW Hya with an inner disk hole of size ~ 4 AU, and hypothesized that a Jupiter-mass planet may have formed there. Similar conclusions have been drawn for the Taurus objects GM Aur (Rice et al. 2003; Bergin et al. 2004; Calvet et al. 2006), DM Tau (Bergin et al. 2004; Calvet et al. 2006) and CoKu Tau/4 (Forrest et al. 2004; Quillen et al. 2004; D’Alessio et al. 2005), though the latter has subsequently been found to harbor a stellar companion (Ireland & Kraus 2008). Follow-up observations at high spatial resolution have directly confirmed the presence of holes or gaps in a few disks (Hughes et al. 2007; Ratzka et al. 2007; Brown et al. 2008; Hughes et al. 2009). However, the overall frequency of transition objects as a function of stellar age, mass, and environment has remained largely unconstrained.

With its superior mid-infrared sensitivity and spatial resolution, the *Spitzer* Space Telescope has begun to address questions of disk evolution and lifetimes and the connection to planet formation in unprecedented detail. *Spitzer* observations taken with the IRAC and MIPS instruments are providing SEDs from 3.6 to 24 μm for large numbers of pre-main sequence stars in star forming regions and young clusters, allowing statistical studies of circumstellar disk evolution through the properties of dust emission as a function of stellar age, mass, and environment (Lada et al. 2006; Sicilia-Aguilar et al. 2006; Hernández et al. 2007, Balog et al. 2007; Kennedy & Kenyon 2009, among many others). Here we report on the statistics of transition disks as identified from *Spitzer* SEDs for stars in nearby young regions, providing the first robust statistics of disks with inner holes around stars in young stellar clusters and associations with ages 1-10 Myr.

2. Observations and Sample

We have culled disk candidates from 7 regions observed as part of existing *Spitzer* GTO and GO surveys of young clusters and star forming regions. The sample is listed in Table 1. We included only regions within about 400 pc so as to optimize completeness limits, particularly at longer wavelengths, and restricted to mean stellar ages of 10 Myr or less. The sample includes four clusters with active star formation, and three older stellar associations where star formation has ceased (and the natal molecular material has been

¹The “transition disk” terminology is somewhat subjective and has a wide range of definitions in the literature. For the purposes of this paper, we define a “classical” transition disk specifically as an optically thick protoplanetary disk with an \sim AU-scale inner region that is optically thin or completely evacuated of small dust grains. We alternately refer to these as disks with inner holes.

swept away). Some transition objects in some of these regions have already been reported in the literature; however, the nomenclature and methodology varies widely. Our aim here is to narrowly define transition disks and provide complete statistics by using a consistent selection method for identifying them.

Each region was mapped with both the IRAC and MIPS instruments, with total coverage ranging from 30'x30' to 60'x60'. Data from each instrument are separated in time by a few weeks to a few months; however, all channels within each instrument were obtained simultaneously. We defer the details of data processing, mosaicking, and photometry to separate papers on each of the regions, referenced in Table 1. We do not consider data from the 70 or 160 μm channels of MIPS here because of severe incompleteness and saturation effects. The *Spitzer* sources were matched with 2MASS data, and the 2MASS coordinates were adopted in each case (all the disk candidates discussed here have a matching 2MASS source detected at *J*, *H*, and *K*).

3. Results

3.1. SED classification

We have selected circumstellar disk candidates from each region based on spectral slope measurements across the IRAC and MIPS 24 μm channels. The spectral slope provides a useful means of distinguishing between stars with and without infrared excess emission from circumstellar dust, and can also be used to distinguish rough evolutionary characteristics (e.g. Lada et al. 2006; Hernández et al. 2007; Flaherty & Muzerolle 2008). We focused on two different wavelength intervals, 3 to 5.8 μm and 8 to 24 μm , in order to sample dust at two different temperature regimes (and hence locations in the disk). Figure 1 shows these slope values for the 7 regions in our sample (data from the Orion OB1a and b associations have been combined in one panel). Sources clustered at $\alpha_{8-24} \sim -3$ represent bare photospheres with little or no excess dust emission. The locus of points in the range $0 \leq \alpha_{8-24} \leq -1$, $-1.8 \leq \alpha_{3-5} \leq 0$ are objects with optically thick circumstellar disks. Many of these have been confirmed with follow-up optical spectroscopy as being T Tauri stars.

We lack complete membership confirmation for three of the clusters (NGC 1333, L 1688, NGC 2068/2071). Other non-PMS objects can exhibit similar spectral slopes from dust excess, mainly high-redshift galaxies and AGN and background AGB stars. Since the vast majority of background objects are faint, we attempted to limit the contamination for those three clusters by applying a magnitude cut of $[3.6] < 14.5$. We applied a further cut using $[4.5] - [8]$ and $[5.8] - [8]$ color criteria from Winston et al. (2007) and Gutermuth

et al. (2008) to remove star forming galaxies and AGN with strong PAH emission. Based on extragalactic source counts and observations of galactic fields which lack young stellar objects, we estimate the final level of contamination in the disk locus to be very low, of order 1% or less (see also Gutermuth et al. 2008). In any case, contamination is not an issue for the other four regions, which have extensive published membership information, and we consider confirmed members only.

It is apparent in Figure 1 that there are a handful of sources with flat or increasing slopes from 8-24 μm but sharply declining (near-photospheric) slopes at 3-5 μm . Such behavior is indicative of optically thick dust emission at the longer wavelengths but very small or no dust excess at the shorter wavelengths. For typical T Tauri-type disks, emission at 4.5 μm probes dust at distances of ~ 1 AU from the central star. Thus, the lack of excess emission at the shorter wavelengths points to an optically thin or evacuated (at least of small grains) “hole” in the disk at those radii, while optically thick material exists further out at $\gtrsim 1$ AU. For comparison, the spectral slopes for three well-studied transition disks (see Table 2) are also shown in Figure 1. For selecting inner disk hole candidates, we then adopted a spectral slope locus based on these previously known objects, with thresholds $\alpha_{3-5} < -1.8$ and $\alpha_{8-24} > 0$. The former criterion roughly corresponds to the maximum slope value for reddened background stars, and is also similar to values applied previously to separate “normal” accretion disk emission from more evolved or optically thin disk emission (e.g. Lada et al. 2006; Hernández et al. 2007; Flaherty & Muzerolle 2008). Those studies calculated slopes across the full IRAC wavelength range, 3.6 to 8 μm . We have excluded the 8 μm band in order to avoid artificially large slopes due to strong 10 μm silicate emission, which partially overlaps the 8 μm bandpass, as well as potential contamination from PAH emission in the surrounding molecular cloud material. The longer wavelength criterion was selected to weed out potentially optically thin outer disks; $\alpha_{8-24} = 0$ corresponds to $L_{IR}/L_* \sim 0.05$ in the limit of no 8 μm excess and single-temperature blackbody dust emission. This cutoff also avoids completeness limitations at 24 μm .

SEDs for two transition disk candidates, plus a third object that satisfies only the short wavelength criterion, are shown in Figure 2. The object in the top panel exhibits nearly pure photospheric emission out to 5.8 μm , and a sharp upturn from 8 to 24 μm , as expected. On the other hand, the object in the second panel shows a similar SED shape but has a clear excess above the predicted photosphere at wavelengths as short as 2 μm despite having a steep 3-5 μm spectral index. In this case, the excess emission at $\lambda < 8$ μm is consistent with a single-temperature blackbody of ~ 1400 K (probably dominated by emission from the disk “wall” at the dust sublimation radius; e.g. Muzerolle et al. 2003; Espaillat et al. 2008a), which the spectral index technique is not able to distinguish from blackbody emission typical of a stellar photosphere. The short-wavelength excess emission is significantly reduced from

“typical” T Tauri disks, akin to the “evolved” disks reported by various authors (e.g., Lada et al. 2006; Hernández et al. 2007). However, the interpretation of its origin is more complicated than in the case of truly optically thin or zero excess emission as seen in the top panel of Figure 2, particularly for the lowest mass stars where hot dust generally produces less emission (Ercolano et al. 2009). Finally, the object in the lower panel exhibits no dust emission at $\lambda < 5.8 \mu\text{m}$ but weaker excess at $24 \mu\text{m}$ with no obvious upturn in the long-wavelength continuum. Objects with this type of SED have much lower fractional infrared luminosities, and cannot be reliably distinguished from fully optically thin disks (such as debris disks) with our data alone.

We have attempted to eliminate ambiguous cases from our statistics by estimating the actual amount of excess at $5.8 \mu\text{m}$. This was accomplished by comparing to a predicted photospheric SED and calculating the ratio of observed to predicted flux at the wavelength of interest. In this case, we constructed empirical SEDs as a function of spectral type from the main sequence dwarf colors given by Kenyon & Hartmann (1995). Such a procedure is sensitive to both the spectral type of the object and the amount of extinction it suffers. We culled spectral types and A_V values for all transition candidates from the literature (see Tables 3- 5). Each object SED was dereddened using these A_V values and reddening laws from Flaherty et al. (2007) (for $\lambda = 3.6 - 8 \mu\text{m}$) and Mathis (1990) (all other wavelengths). The observed and photospheric SEDs were then normalized at J where excess emission from dust should be negligible, particularly for these evolved disk candidates. In some cases, the literature A_V values resulted in a poor match between observed and photospheric SED in the near-infrared, with the observed fluxes being systematically lower. In these cases, we used a χ -squared procedure to determine the A_V value that produced the best fit between the observed JHK fluxes and the photosphere template (the change from published values was never more than $\sim 30\%$). The predicted photospheric flux at $5.8 \mu\text{m}$ was then calculated by convolving the IRAC channel-3 bandpass function with a spline fit to the scaled empirical SED.

Figure 3 shows the distribution of observed to predicted $5.8 \mu\text{m}$ flux ratios ($f_{5.8}$) for three subsets of the members of the IC 348 cluster. All objects with no evidence for infrared excess emission at any wavelength based on the spectral slope are distributed around $f_{5.8} \sim 1$, as expected. Objects with $24 \mu\text{m}$ excess but $\alpha_{3-5} < -1.8$ show a broader distribution that peaks around $f_{5.8} \sim 1.5$. This result indicates that most of the transition disks do in fact have non-zero excess emission at this wavelength, probably from optically thin dust (see discussion). By contrast, all but 3 of the objects with $24 \mu\text{m}$ excess and $\alpha_{3-5} > -1.8$ show much larger flux ratios, again as expected. ² By comparing to the flux ratios of the three Taurus reference

²However, we note that the equivalent value of this flux ratio for the Taurus median SED (D’Alessio et

transition disks, and adopting a reasonable boundary between the candidate transition and normal disk flux ratio distributions in Figure 3, we added a final transition disk selection constraint of $f_{5.8} < 1.7$. The final list of classical transition disks is shown in Table 3. The remaining candidates that did not pass the $f_{5.8}$ criterion, indicating larger excess emission in the IRAC wavelength range, are listed in Table 4 as “warm excess” transition disks. Finally, remaining objects that passed the $f_{5.8}$ criterion but exhibited weaker $24 \mu\text{m}$ excess emission ($\alpha_{8-24} < 0$) are listed in Table 5 as “weak excess” transition disks. These last two sets of objects are discussed separately in section 3.3.

3.2. Statistics

We now estimate the frequency of disks with AU-scale inner holes in each of the sample regions. The stellar populations have not been completely characterized in all cases, so a frequency relative to the total number of stars N_* cannot be calculated reliably. However, the total number of objects in each region with excess emission out to $24 \mu\text{m}$ characteristic of optically thick circumstellar disks can be estimated from the *Spitzer* spectral slopes alone. Since contamination from unrelated sources is very low, as estimated above, this number should be a reliable indicator of the total number of protoplanetary disks N_{disk} in each region (at least for most of the stellar mass range; see below). The resulting classical transition disk frequency, expressed as N_{hole}/N_{disk} , is given for each region in Table 1. The fraction of disks with inner holes ranges from about 1% in the youngest, most embedded clusters to 17% in the oldest regions.

Our statistics are potentially biased since the sensitivity at $24 \mu\text{m}$ is not sufficient to detect photospheres for any but the earliest spectral types at the distances of the clusters in the sample. In addition, the bright background emission at $24 \mu\text{m}$ endemic to star formation regions further limits sensitivity, though in a nonuniform manner. The limiting case of a transition disk with no excess at $8 \mu\text{m}$, a spectral slope $\alpha_{8-24} = 0$, and a $24 \mu\text{m}$ flux at the typical completeness limit [24] $\lesssim 9$ roughly corresponds to a 1 Myr-old M5 star at 320 pc. The $24 \mu\text{m}$ limit will be brighter in small regions where the background is strongest and most highly structured, though the effect should be relatively random within a given region since there is no direct correlation between the background emission and the cluster spatial distributions. However, the overall background does vary among the regions of our study.

al. 1999), assuming a K7 photosphere, is about 5.4. That almost all of the IC 348 “normal” disks are below this value further indicates the overall advanced state of disk evolution for this older cluster, as first shown by Lada et al. 2006.

The average brightness and peak-to-valley variations are the most significant in IC 348 and L 1688, somewhat more moderate in NGC 2068/2071, bright but uniform in NGC 1333, and very low in the three older regions.

We can make a more detailed assessment of the completeness with IC 348, which has good number statistics, complete membership, and an intermediate distance for our sample. For all the sources detected at all IRAC bands but not at 24 μm , we selected remaining disk candidates from sources with the appropriate α_{3-5} . There are also many sources with possible excess at only 8 μm . We selected those with the criteria $[5.8] - [8] > 0.1$ and $[5.8] - [8] > 3\sigma_{5.8-8}$. The former cut corresponds to the smallest color in our transition sample, while the latter cut eliminates objects whose photometry has large uncertainties because of strong background emission. We also eliminated all objects with spectral types later than M6.5 since none have 24 μm detections. From these cuts we identified a total of 35 objects with likely excess emission at 8 μm or less. Of these, 6 exhibit $f_{5.8}$ and 24 μm upper limits consistent with being transition disks (though of course many of these could be in our weak excess category). All but two have spectral types M5 or later. Combining with the 24 μm -detected sample, we get a total of 134 objects with circumstellar disks, of which anywhere from 12 to 18 may exhibit mid-IR emission characteristic of optically thick outer disks with AU-scale inner holes. This yields a range in the transition disk fraction of 9 - 13%, within the 1σ confidence interval of our original estimate. We conclude that the statistics we have derived from the 24 μm -detected samples are not significantly biased, and are probably accurate within the uncertainties assuming binomial counting statistics.

3.3. Transition disk properties

3.3.1. Stellar properties and environment

We have spectroscopic information for all 20 of our classical transition disks (Table 3). All of them are confirmed to be *bona fide* pre-main sequence members of their respective clusters/associations on the basis of spectral type, Li absorption, hydrogen line emission, and/or various gravity-sensitive photospheric features (see for instance Luhman et al. 2003 on IC 348 for details of youth and membership criteria). The candidates span a wide range of spectral types, from as early as G1 to as late as M6.5. Given ages of 1-10 Myr based on PMS evolutionary tracks such as Siess et al. (2000) and Baraffe et al. (1998), these spectral types correspond to a mass range of roughly 2.5-0.1 M_{\odot} . One object in IC 348 is a likely brown dwarf ($M = 0.06 M_{\odot}$ according to the Baraffe tracks), and was presented in more detail in Muzerolle et al. (2006). The distribution of spectral types is shown in Figure 4. For the sample as a whole, the number of transition objects rises from G1 to \sim M5, and then drops

off sharply thereafter (probably reflecting the completeness limit of the *Spitzer* observations). For comparison, the stellar IMF from Kroupa (2001) is also shown in Figure 4; stellar mass was converted into spectral type using the Siess et al. (2000) pre-main sequence tracks and the effective temperature scale given by Kenyon & Hartmann (1995). There appears to be a deficit of M-type stars with classical transition disks compared to the IMF, although the small sample size makes a quantitative statistical comparison difficult. We conclude that there is some evidence that the kind of inner disk clearing behavior traced by our sample may have a stellar mass dependence, where objects with $M \lesssim 0.3M_{\odot}$ are less likely to exhibit a transition SED.

There is a hint of a spectral type dependence in our sample as a function of age. The three youngest regions lack any transition disks around stars later than M1, while the transition sample in the four older regions is dominated by mid-M spectral types. Despite the small statistics, we believe this may be a robust result since the parent population of spectral types of stars around which we can detect disk emission out to $24 \mu\text{m}$ for each cluster peaks strongly at about M4-M5. An apparent counter-example to this possible age dependence is the 10 Myr-old TW Hydrae association, which has three transition objects all with spectral types earlier than M4 (Table 2). However, the median spectral type of the total sample of ~ 20 confirmed stellar members (Webb et al. 1999; Sterzik et al. 1999; Zuckerman et al. 2001) is M1, and there is only one known stellar member later than M3.5, reflecting either a bias from the X-ray and proper motion techniques used to identify members or an anomalous initial mass function (Moraux et al. 2007). In any case, we cannot draw definitive conclusions without a larger sample. However, we do note that studies of the overall disk frequency show a similar mass-age dependence where more massive stars tend to lose their disks earlier (Lada et al. 2006; Carpenter et al. 2006; Kennedy & Kenyon 2009).

We also looked for signs of accretion activity in these disks using spectroscopic indicators such as emission lines. Quiescent (“passive”) or accreting disks can be crudely distinguished on the basis of $\text{H}\alpha$ emission equivalent width. Adopting the spectral type-dependent criteria of White & Basri (2003), we can separate chromospheric from accretion emission for all objects with $\text{H}\alpha$ measurements (Table 3). We find that 9/17 classical transition disks in our sample show evidence for active accretion. This may be a lower limit since much of the $\text{H}\alpha$ data are based on low-resolution spectra; some weak accretors can exhibit line equivalent widths below the adopted threshold yet still show signposts of gas infall in velocity-resolved line profiles (e.g. Flaherty & Muzerolle 2008). High spectral resolution observations for some objects have been reported in the literature, and we mark them in Table 3. None of the accretor classifications change as a result, but we point out that all but one of the “non-accretors” have yet to be observed at high resolution and remain untested. High-resolution spectroscopy of $\text{H}\alpha$ for the full sample is required to obtain the best constraints on any

residual accretion activity. Even with velocity-resolved data, all quoted accretor fractions should be considered lower limits, since very weak accretion may not produce any observable diagnostic. In any case, for accretion to occur, gas must be present in these disks very close to the star (< 0.1 AU). Thus, the appearance of accretion signatures in over half of the transition objects with spectroscopic information indicates that the presence of gas in the inner optically thin regions of transition disks is surprisingly common.

To test for any effect of environment on the clearing of inner disk holes, we compared the spatial distribution of our transition disk sample. We did not include the three older associations, since they are more diffuse and the *Spitzer* coverage of their total membership is likely incomplete. The four younger clusters are all primarily low-mass star forming regions (no O stars, only one or two B stars) and have similar stellar densities. Figure 5 shows the distribution of fifth-nearest neighbors for the transition disks versus all other disks for the combined cluster sample. As advocated by Gutermuth et al. (2005), the fifth-nearest neighbor statistic should be a reasonable compromise, weeding out statistical outliers and wide binaries while still accounting for non-spherical substructure common in young clusters. Although the small numbers prevent a reliable quantitative statistical test, there is no obvious difference between the two distributions. This suggests that whatever process controls the transition phase is not directly linked to either local stellar density or radiation environment, at least in the rather limited range probed by the clusters considered here.

Stellar multiplicity is another important property that can have a significant effect on inner disk clearing. Close companions can clear a hole in the circumbinary disk, as in the case of CoKu Tau/4, while wide companions may have an indirect influence on circumprimary disk evolution. We unfortunately have little information concerning the multiplicity of the transition sample. None of the objects have resolved companions in either the 2MASS or IRAC images, which places separation limits of roughly $a < 320 - 800$ AU depending on the distance. This is not very stringent since the majority of known young binary systems have smaller separations. Only two of the sample regions, IC 348 and η Cha, have been subject to extensive high spatial resolution binary searches. In the case of IC 348, Duchêne et al. (1999) observed transition objects LRL 21, 67, and 133, and found no companions with mass ratio $q \gtrsim 0.1$ and separation $a \gtrsim 50$ AU; none of the other transition objects were observed. For the η Cha association, Brandeker et al. (2006) found no companion with mass ratio $q \gtrsim 0.1$ and separation $a \gtrsim 20$ AU around the transition object RECX 5. Finally, a recent VLBA study of DoAr 21 in L 1688 detected a stellar companion with separation of roughly 1.5 AU (Loinard et al. 2008).

3.3.2. Age trend

There is some indication of a possible trend with age, in that the three youngest clusters in our sample have a significantly lower classical transition disk fraction (f_{hole}) than the other four regions. Some of this trend might be a result of the overall decline in total disk fraction (f_{disk}) with time (see the upper panel of Figure 6), since we have calculated f_{hole} relative to the disked rather than total stellar population of each cluster. We can estimate N_{hole}/N_* if f_{disk} is known and assuming that our transition disk sample is complete. The disk fraction has been estimated from *Spitzer* data for most of the regions in our sample: NGC 1333 (83%; Gutermuth et al. 2008), NGC 2068/2071 (75%; Flaherty & Muzerolle 2008), IC 348 (47%; Lada et al. 2006), η Cha (40%; Megeath et al. 2005), and Orion OB1a and b (6% and 13%, respectively; Hernández et al. 2007). We then derive $N_{hole}/N_* \sim f_{trans} \times f_{disk} \sim 1.2^{+3.0}_{-1.0}$, $1.5^{+1.4}_{-0.8}$, $5.6^{+2.4}_{-2.2}$, $1.0^{+2.0}_{-0.8}$, $6.6^{+11}_{-6.4}$, and $1.0^{+1.8}_{-1.0}$ % for the 7 regions in order of increasing age. These percentages are clearly not equal, although the age trend is not well-defined or consistent. Further observations of other regions in the crucial 3-10 Myr age range are needed to improve the statistics. We do emphasize that there are biases that can effect these estimates. We have already discussed detection limits. Also, assigning ages to young stars is fraught with complications, being model dependent and subject to significant biases from variability and accretion effects and uncertain age spreads (at least within a few Myr) among individual objects. We have chosen to make qualitative comparisons based on mean ages for each region rather than adopting ages for individual objects. It is possible the transition objects are systematically older than the mean age of the clusters, but we find no statistically significant evidence of a such a bias in the HR diagrams of these regions.

If the trend with mean age is real, it may reveal important clues to the mechanisms that create the inner disk clearing and the eventual dissipation of the entire disk. We looked at this in more detail by constructing a parametric model of disk dissipation using Monte Carlo techniques. The observed decline in f_{disk} with time can be used to trace the overall disk dissipation rate. We have collected all estimates of f_{disk} from *Spitzer* observations of young clusters and associations, and show them in the upper panel of Figure 6. All but one of these estimates is based on the presence of excess emission at $\lambda \leq 8 \mu\text{m}$ from IRAC imaging data; the exception is the TW Hydrae association, for which we estimated f_{disk} from the MIPS data in Low et al. (2006), selecting all objects with $L_{IR}/L_* \gtrsim 0.1$ indicative of optically thick disks. Most of the regions are near enough ($d \lesssim 500$ pc) for the disk inventories to be complete down to or below the substellar limit. We see a clear decline with age with relatively small scatter – the only significant outliers are Tr 37 at $t \sim 4$ Myr and η Cha at $t \sim 7$ Myr; the former likely contains a mixed stellar population from separate star formation episodes (Sicilia-Aguilar et al. 2004), while the latter has only 15 known members and may have been subject to significant dynamical evolution. The drop in f_{disk} is initially

quite rapid, down to $\sim 40\%$ by 3 Myr, then appears to tail off into a more gradual decline at older ages.

Based on these observations, we adopted a two-component parameterization to describe the disk dissipation rate for our model. The exact functional form, and a physical motivation for it, is not important here; we do note that a single exponential decay cannot match the observed tail at 5-10 Myr. The resulting simulated disk fraction at each time step from $t = 0$ to 10 Myr, assuming an initial disk fraction of 100%, was calculated for an ensemble of 10^5 stars. We adopted a gaussian age distribution with $1\sigma \sim 1$ Myr centered at t for the ensemble to reflect the typical small age spread in young clusters. Finally, we assumed that as each disk dissipates, it immediately forms an AU-scale inner dust hole and remains in that state for a time t_{hole} , during which the disk exhibits our defined transition characteristics and after which all disk material detectable out to $24 \mu\text{m}$ has completely dissipated. We then varied t_{hole} to best match the observed transition disk fraction (lower panel of Fig. 6). A value of $t_{hole} = 0.1$ Myr, similar to previous estimates derived from simple statistical arguments, results in an order-of-magnitude agreement. The actual number of transition disks in the simulated ensemble is constant with time within each of the two decay intervals (0–3, 3–10 Myr), since we assume a constant decay slope. The rise in the model f_{hole} from 0-2 and 5-10 Myr is a consequence of the decrease in the total disk fraction, while the dip at 2-5 Myr is produced by the “elbow” between the two decay intervals where the adopted decay slope changes. However, the model does not reproduce the data in detail; it slightly overpredicts f_{hole} at 1-3 Myr, and underpredicts f_{hole} at 3-10 Myr.

Better agreement with the data might be accomplished by adopting an age-dependent t_{hole} . Figure 6 shows a second model with $t_{hole} = 1$ Myr (the decay rates were adjusted in this case in order to match the observed f_{disk} , otherwise the model would vastly overpredict the disk fraction at 1-3 Myr); this model provides a good match to observations at 5-10 Myr. Alternatively, it is possible that only a fraction of the disks that dissipate at $t \lesssim 3$ Myr actually go through an identifiable transition phase, while the rest dissipate much more quickly through other means (e.g. disruption from encounters or binary interactions). This dichotomy may also be related to the spectral type dependence indicated in Figure 4, which our simple model does not take into account. A more sophisticated model awaits better characterization of mass-dependent disk dissipation rates. We can estimate this in a very rough way by considering two spectral type bins: K0-M1, which encompasses all of the young (1-2 Myr) transition objects, and M1-M5, which encompasses most of the older (3-10 Myr) transition objects. The fraction of all cluster stars in each bin, assuming a typical IMF, is roughly 30% and 70%, respectively. Since the young transition disks are only in the early-type bin, while all young disks span the full range of spectral types, we can estimate an “IMF-weighted” transition disk fraction of $0.02/0.3 = 7\%$ at 1-2 Myr. This is closer to

the 7-17% range at 3-10 Myr, although an absolute age dependence cannot be confidently ruled out. In any case, our results may indicate that different disk dissipation mechanisms may operate at different times. Specific physically-motivated models are needed to explore this in more detail. In addition, more data in the 5-10 Myr age range are needed to better constrain the age trend; unfortunately, statistics will be hard to come by since the overall disk fractions are so small at older ages.

3.4. Warm and weak excess transition objects

The remaining sources flagged as possible transition disks by their spectral slopes but rejected based on other criteria are nevertheless interesting since they still exhibit some signs of significant evolution. The warm excess sources show some continuum excess emission at $\lambda = 3 - 8 \mu\text{m}$ that, while in many cases may be optically thick, is still significantly below “typical” disk emission at those wavelengths. Meanwhile, the spectral slope at 8-24 μm increases steeply in all cases. These SED dips may indicate a substantial lack of dust at disk radii somewhere outside of the dust sublimation radius but within about 1-20 AU. Similar behavior has been recently reported in a number of disks around nearby young solar-type stars (Brown et al. 2007) and 3 stars in Taurus (Espaillat et al 2007). Radiative transfer models of these objects are able to reproduce their SEDs by including substantial disk gaps with inner radii $R \sim 0.1 - 2$ AU and outer radii $R \sim 5 - 50$ AU. Hence, these objects may be precursors to an inner hole phase (so-called “pre-transitional” disks; Espaillat et al. 2007). Interestingly, the fraction of measurable accretors in this group (5/6; Table 4) is larger than in the classical and weak excess transition categories (though admittedly the sample size is very small). Two of these objects have $\text{H}\alpha$ equivalent widths below the adopted threshold, but one (FM 326) does show a weak accretion component in the line profile at high spectral resolution (Flaherty & Muzerolle 2008). Note that the single non-accretor has not been observed at high spectral resolution, so it is possible that all six of these sources are still accreting.

The weak excess sources have mid-IR fluxes that suggest marginally optically thick if not optically thin disk material at the radii probed by that wavelength. It is possible that some of these SEDs might rise at $\lambda > 24 \mu\text{m}$, indicating very large inner holes. One such object in the nearby Lupus star forming region was discovered by Padgett et al. (2006), although its fractional disk luminosity of $\sim 8 \times 10^{-4}$ suggests its outer disk may be optically thin. One of our sources, FM 458, is coincident with a bright MIPS 70 μm (Flaherty & Muzerolle 2008) and SCUBA sub-mm source (Mitchell et al. 2001). However, the long-wavelength luminosity suggests a very large mass of circumstellar material, and the source

may be a chance superposition of a T Tauri star with a Class 0/I object. In any case, the *Spitzer* data generally lacks sufficient sensitivity at $70\ \mu\text{m}$ (because of the greater distances and much stronger background emission) for better statistics on any disks with extremely large inner holes.

There are two characteristics of note for the weak excess sample. First, their accretion activity appears to be significantly reduced if not absent. Only 3/20 objects exhibit $\text{H}\alpha$ equivalent widths above the accretion threshold. Again, we could be missing some weak accretors since high spectral resolution observations are lacking for most of the sample. Broad and/or asymmetric line profiles suggestive of weak accretion have been observed in three objects, FM 458 and FM 998 (Flaherty & Muzerolle 2008) and RECX 9 (Lawson et al. 2004), which brings the accretor fraction to 6/20, or $\sim 30\%$. Nevertheless, in comparison with the classical and warm excess transition objects, the relative $\text{H}\alpha$ strengths indicate that the weak excess sources are more weakly accreting on average. Second, these sources are strongly associated with lower mass stars; 20/25 have spectral types later than M0, and the distribution of types rises sharply to our completeness limit of M4-M5. This behavior may be analogous to the passive disks reported by McCabe et al. (2006), which showed weak/absent accretion and appeared only around M stars. Figure 7 shows the spectral type distribution of the combined transition sample. In marked contrast to the classical transition sample, the combined distribution strongly peaks at later spectral types, and is much more consistent with the stellar IMF. Since the weak excess objects with mid-M types are more likely to be affected by detection biases because of their weaker $24\ \mu\text{m}$ fluxes, the combined distribution further bolsters the argument that the classical transition objects may be underrepresented among mid- to late-M stars.

The trend of increasing transition disk fraction with age is greatly enhanced if the warm and weak excess sources are included. In that case, we would get 1.5% (1/66), 2.7% (2/74), 6.6% (10/152), 26% (26/99), 29% (4/14), 67% (4/6), and 67% (4/6) for the 7 regions in our study in rough age order (see Fig. 6). These statistics are less robust since the weak excess sample is likely not complete, particularly for the more distant young clusters with higher background emission. Nevertheless, there is a clear trend of increasing frequency of highly evolved disks as a function of age, as has been seen by prior studies looking at spectral slope evolution.

4. Discussion

Understanding the properties of circumstellar disks with significant dust clearing in their inner regions may have profound implications for planet formation processes. If indeed

these transition disks are showing us the end-stages of protoplanetary disks, their statistics are indicative of disk dissipation mechanisms and timescales, which can then be used to constrain models of planetesimal growth and/or giant planet accretion. Some of the objects in our sample have ages of 1 Myr or less, which implies that the disk clearing mechanism(s) must operate very quickly. Our simple parametric model of disk dissipation indicates a characteristic “transition” time in the range $0.1 - 1 \times 10^6$ years, possibly dependent on the stellar age and/or mass. There have been competing claims in the recent literature regarding the transition timescale, with some advocating for a rapid transition of order 10^5 years (e.g., Furlan et al. 2009) and others arguing for a much longer timescale comparable to the stellar age (e.g., Sicilia-Aguilar et al. 2008; Currie et al. 2009ab). Much of the discrepancy may lie in the wide range of adopted definitions of what constitutes a transitional disk; the studies that derive longer transition times tend to use much less restrictive selection criteria. Our results support a slower transition for disks only around stars older than ~ 3 Myr. As we mentioned in section 3.3.2, it is difficult to directly compare statistics for regions of different ages because they also appear to probe different stellar mass regimes. This uncertainty can only be addressed once the dependence of disk evolution on stellar mass has been better-delineated. All of the transition times were estimated assuming that every disk goes through the same inner hole phase. However, our observation of a possible deficit of classical transition disks around late-type stars, as well as the apparent age dependence of the transition disk frequency, appears to contradict this assumption. If classical transition disks do not represent a universal phase of disk evolution, then the clearing timescale may be longer than our estimates.

The presence of accretion, and hence gas within the dust hole, in a majority of the classical transition objects presents challenges to understanding how the inner disk is cleared of small grains while the outer disk (given the significant excesses at $\lambda > 10 \mu\text{m}$) is not. One possibility is that significant grain growth to meter-size or larger bodies has occurred in the inner disk, as has been suggested by models of grain coagulation (Weidenschilling 1997; Dullemond & Dominik 2005). However, some other process is then needed to decouple the outer disk so that accretion from there cannot replenish the supply of small grains to the inner disk. In this scenario, the inner disk should then drain onto the star in a viscous time, which for typical T Tauri parameters is of order a few 10^5 years, similar to some of the clearing timescales estimated above. Several gap-creating mechanisms have been proposed for T Tauri disks, including photoevaporative mass loss induced by UV radiation from the central star (e.g., Clarke et al. 2001) and the dynamical influence of a giant planet (e.g., Bryden et al. 1999). Najita et al. (2007) review these mechanisms and suggest that no single one operates in all cases. Our results support this view, particularly if the hole clearing timescale or incidence really does vary with stellar age and mass. The weak excess transition

objects may represent a stronger case for the photoevaporation mechanism: the low or absent accretion activity and low disk masses as implied by the small fractional infrared excess are both properties predicted by the models at the time of inner hole formation (see also Cieza et al. 2008). However, the large number of these objects, especially at older ages, may not be consistent with photoevaporation model predictions that the outer disk should dissipate very rapidly following inner hole formation (less than 10^5 years; Alexander et al. 2006). This may be resolved if photoevaporation is less efficient for M stars; current models have not yet fully explored the effect of stellar mass.

The inner disk clearing we see in the accreting transition objects (if not all of them) is most likely due to an advanced stage of dust evolution, either from growing planetesimals or possibly newly formed planets. Such processes occur across a large range of ages, from the youngest ~ 1 Myr embedded star forming regions to some of the oldest known classical T Tauri stars such as the 10 Myr-old TW Hya, with some evidence for an increasing frequency with age. The cause of such disparate onset times for inner disk clearing is a key question that remains unanswered. Initial conditions, such as the initial disk size and mass, may play a role. For example, disks of the same mass that are born with different initial sizes will viscously evolve at different rates, may form planets at different times, and may have different susceptibility to photoevaporation. All of these properties can influence the onset time of inner clearing and the amount of time required for the outer disk to dissipate. More massive stars may be born with more massive disks, which might have the best chance for forming giant planets. Such a scenario could explain the young transition disks, which are preferentially associated with more massive stars. It may also explain the deficit of classical transition disks around the lowest mass stars, if in fact photoevaporation turns out not to be an efficient gas removal mechanism. Alexander & Armitage (2009) have explored some of these parameters by calculating disk evolution models including the effects of giant planet formation, migration, and photoevaporation. Interestingly, the transitional disk fraction they predict as a function of stellar age is qualitatively similar to our observed trend (although their values at 5-10 Myr are somewhat higher). However, they used a solar-mass star for all models, so the stellar mass dependence remains to be considered.

We have shown that most classical transition disks exhibit trace amounts of excess emission at $5.8 \mu\text{m}$, indicating that the inner holes are not totally devoid of small grains. This is consistent with models of *Spitzer*-IRS spectra of transition disks published to date, which can only explain the observed $10 \mu\text{m}$ silicate emission in most cases by placing optically thin dust inside the hole (e.g. Calvet et al. 2005). The origin of this dust is unclear. It is possible that in objects that are still accreting, some dust is entrained in the accretion flow passing from the outer disk into the hole; numerical simulations by Rice et al. (2006) of a disk gap cleared by a giant planet show that pressure gradients at the outer edge of

the gap can filter dust particles, allowing only small grains to pass through the gap along with the gas accretion flow. However, many of the non-accreting transitional systems also show hot dust excess, although some of these may be accreting at rates too low to produce observable diagnostics. Some objects, particularly those with larger $f_{5.8}$, may still have optically thick material near the dust sublimation radius. In that case, the emission may have been reduced from that of typical disks because of a lower scale height brought about by dust grain growth and settling. An asymmetric inner disk geometry such as a warp might also produce lower excess emission at certain orientations; this may manifest itself through mid-infrared variability, which has been recently discovered in the transitional disk LRL 31 (Muzerolle et al. 2009). Finally, there may also be *in situ* dust production via colliding planetesimals, as Eisner et al. (2006) proposed for TW Hya, possibly tracing active terrestrial planet formation.

One obvious question is whether the three classes of evolved disks identified here are connected. We would argue that the classical and warm excess transition objects do likely represent an evolutionary sequence. The warm excess sources are akin to the pre-transitional disks described by Espaillat et al. (2007), and are most likely produced as a result of embedded giant planets carving out large gaps in the disks (Espaillat et al. 2008). As the planet continues to grow via accretion from the outer disk, it should eventually stifle accretion through the gap and onto an optically thick inner disk, which may render the interior completely optically thin and result in a classical transition disk. However, the link between these and the weak excess disks is much more dubious. The sheer numbers of the weak excess objects, particularly around older stars, are too great to simply be the result of further evolution of the outer disks of classical transition objects. The spectral type distributions are also distinctly different. Other studies have suggested that there may be separate disk evolutionary pathways (e.g. Lada et al. 2006; Cieza et al. 2007) of which the different disk classes may be representative. However, the weak excess category is less well-defined, and very likely contains a mixture of different disk types. The identification of true inner holes is not as robust for the weak excess disks around lower mass stars, as recently pointed out by Ercolano et al. (2009). They may instead represent evolution without a cleared inner hole phase. Similar objects have been dubbed “homologously depleted” (Wood et al. 2002; Currie et al. 2009b), suggesting that the dust opacity has been reduced through grain growth and mass loss across a wide range of disk radii. We would like to point out that dust grain growth and settling acts to shrink the effective range of disk radii probed at a given wavelength; the models of D’Alessio et al. (2006) show that the majority of dust emission at $25 \mu\text{m}$ is located within $\sim 1 - 2$ AU in a highly settled disk. Thus, radial dust evolution in these disks cannot be definitively ruled out without measurements at far-infrared wavelengths. It is also very possible that some of the weak excess transition disks may in

fact be recently-formed debris disks; further study of their gas content is required before this distinction can be made.

The recent discovery that the CoKu Tau/4 disk is circumbinary (Ireland & Kraus 2008) has fueled speculation as to whether all transitional disks are in fact the result of disk clearing by a stellar companion, and indeed whether such objects are truly transitional. We argue that regardless of hole formation mechanism, all objects showing these SED characteristics are likely to be in transition. There are examples of close binaries whose SEDs betray no evidence for significant inner holes (DF Tau, separation ~ 13 AU, and GW Ori, separation ~ 1 AU, to name a few), which suggests that disks around close binary systems can and do evolve in a similar fashion.

Unfortunately, we lack binary statistics for our sample, particularly at close separations (< 10 AU). We can indirectly assess the importance of binaries by comparing the expected fraction of binaries with our observed transition disk statistics as a function of stellar age and mass. From the multiplicity study by Sterzik & Durisen (2004), we estimate a total multiplicity fraction of about 50% for solar-mass stars, and roughly 20% at $0.2 M_{\odot}$. Since our transition disk selection is sensitive to maximum inner disk hole sizes of roughly 40 AU for solar type stars and 4 AU for low mass stars, any stellar companions must be within this range in order to produce the disk clearing. According to Sterzik & Durisen (2004), about 50% of the $1 M_{\odot}$ binaries have separations < 40 AU while about 30% of the $0.2 M_{\odot}$ binaries will have separations within 4 AU, leading to combined fractions of 25% and 6%, respectively. These estimates are inconsistent with the transition disk statistics in both magnitude and trend with mass, thus we suggest that stellar companions are unlikely to be a significant contributor. Nevertheless, sensitive searches for close stellar companions, both with AO imaging and radial velocity monitoring, need to be done before firm conclusions can be made.

Finally, the possibility of different disk decay rates at different stellar ages, as indicated in Figure 6, is very intriguing in its own right. It may be a further indicator that different disk dissipation mechanisms operate preferentially at different times. The stellar mass dependence, where disks around less massive stars tend to last longer, may also be involved. For example, if either photoevaporation or planet formation is less effective in mid- to late-M stars, their disks may take longer to completely erode. Alternatively, stellar multiplicity may have an effect; evidence suggests that disks tend to disappear more quickly around binaries (e.g. Bouwman et al. 2006), and these may represent the faster decay rate at younger ages. However, counter-examples (long-lived disks around binaries, short-lived disks around single stars) are plentiful. More work needs to be done to fully elucidate the effects of these parameters, as well as others such as environment and initial conditions.

This work is based on observations made with the *Spitzer Space Telescope*, which is operated by the Jet Propulsion Laboratory, California Institute of Technology under NASA contract 1407. We also used data from the Two Micron All Sky Survey (2MASS), a joint project of the University of Massachusetts and the Infrared Processing and Analysis Center (IPAC)/California Institute of Technology, funded by NASA and the National Science Foundation. We thank an anonymous referee for constructive and insightful suggestions. Support for this work was provided by NASA through Contract Number 960785 issued by JPL/Caltech.

REFERENCES

- Alexander, R. D., Clarke, C. J., & Pringle, J. E. 2006, *MNRAS*, 369, 229
- Alexander, R. D. & Armitage, P. J. 2009, *ApJ*, 704, 989
- Balog, Z., Muzerolle, J., Rieke, G. H., Su, K. Y. L., Young, E. T., & Megeath, S. T. 2007, *ApJ*, 660, 1532
- Baraffe, I., Chabrier, G., Allard, F., & Hauschildt, P. H. 1998, *A&A*, 337, 403
- Bergin, E., Calvet, N., Sitko, M. L. et al. 2004, *ApJ*, 614, L133
- Boss, A. P. 1997, *Science*, 276, 5320, 1836
- Bouvier, J. & Appenzeller, I. 1992, *A&AS*, 92, 481
- Bouwman, J., Lawson, W. A., Dominik, C., Feigelson, E. D., Henning, T., Tielens, A. G. G. M., Waters, L. B. F. M. 2006, *ApJ*, 653, L57
- Brandeker, A., Jayawardhana, R., Khavari, P., Haisch, K. E., & Mardones, D. 2006, *ApJ*, 652, 1572
- Briceño, C., Calvet, N., Hernández, J., Vivas, A. K., Hartmann, L., Downes, J. J., & Berlind, P. 2005, *AJ*, 129, 907
- Briceño, C., Hartmann, L., Hernández, J., Calvet, N., Vivas, A. K., Furesz, G., & Szentgyorgyi, A. 2007, *ApJ*, 661, 1119
- Brown, J. M., Blake, G. A., Dullemond, C. P. et al. 2007, *ApJ*, 664, L107
- Brown, J. M., Blake, G. A., Qi, C., Dullemond, C. P., & Wilner, D. J. 2008, *ApJ*, 675, L109
- Calvet, N., D’Alessio, P., Hartmann, L., Wilner, D., Walsh, A. & Sitko, M. 2002, *ApJ*, 568, 1008
- Carpenter, J. M., Mamajek, E. E., Hillenbrand, L. A., & Meyer, M. R. 2006, *ApJ*, 651, L49
- Cieza, L., Padgett, D. L., Stapelfeldt, K. R. et al. 2007, *ApJ*, 667, 308

- Cieza, L. A., Swift, J. J., Mathews, G. S., & Williams, J. P. 2008, *ApJ*, 686, L115
- Currie, T. & Kenyon, S. J. 2009a, *AJ*, 138, 703
- Currie, T., Lada, C. J., Plavchan, P., Robitaille, T. P., Irwin, J., & Kenyon, S. J. 2009b, *ApJ*, 698, 1
- D’Alessio, P., Calvet, N., Hartmann, L., Lizano, S., & Cantó, J. 1999, *ApJ*, 527, 893
- D’Alessio, P., Hartmann, L., Calvet, N. et al. 2005, *ApJ*, 621, 461
- D’Alessio, P., Calvet, N., Hartmann, L., Franco-Hernández, R., & Servín, H. 2006, *ApJ*, 638, 314
- Dahm, S. E. 2008, *AJ*, 136, 521
- Dahm, S. E. & Carpenter, J. M. 2009, *AJ*, in press
- Dahm, S. E. & Hillenbrand, L. A. 2007, *AJ*, 133, 2072
- Duchêne, G., Bouvier, J., & Simon, T. 1999, *A&A*, 343, 831
- Dullemond, C. P. & Dominik, C. 2005, *A&A*, 434, 971
- Eisner, J. A., Chiang, E. I., & Hillenbrand, L. A. 2006, *ApJ*, 637, L133
- Ercolano, B., Clarke, C. J., & Robitaille, T. P. 2009, *MNRAS*, in press
- Espaillet, C. et al. 2007a, *ApJ*, 664, L111
- Espaillet, C. et al. 2008a, *ApJ*, 682, L125
- Espaillet, C. et al. 2008b, *ApJ*, 689, L145
- Flaherty, K. M. & Muzerolle, J. 2008, *AJ*, 135, 966
- Flaherty, K. M., Pipher, J. L., Megeath, S. T., Winston, E. M., Gutermuth, R. A., Muzerolle, J., Allen, L. E., & Fazio, G. G. 2007, *ApJ*, 663, 1069
- Furlan, E. et al. 2006, *ApJS*, 165, 568
- Furlan, E. et al. 2007, *ApJ*, 664, 1176
- Furlan, E., et al. 2009, *ApJ*, 703, 1964
- Gautier, T. N., Rebull, L. M., Stapelfeldt, K. R., & Mainzer, A. 2008, *ApJ*, in press
- Gutermuth, R. A., Megeath, S. T., Muzerolle, J., Allen, L. E., Pipher, J. L., Myers, P. C., & Fazio, G. G. 2004, *ApJS*, 154, 374
- Gutermuth, R., Megeath, S. T., Pipher, J. L., Williams, J. P., Allen, L. E., Myers, P. C., & Raines, S. N. 2005, *ApJ*, 632, 397
- Gutermuth, R., Myers, P. C., Megeath, S. T. et al. 2008, *ApJ*, 674, 336

- Hartmann, L., Megeath, S. T., Allen, L. E., Luhman, K., Calvet, N., D’Alessio, P., Franco-Hernandez, R., & Fazio, G. 2005, *ApJ*, 629, 881
- Hernández, J., Calvet, N., Briceño, C., et al. 2007, *ApJ*, 671, 1784
- Hernández, J., Hartmann, L., Megeath, S. T., et al. 2007, *ApJ*, 662, 1067
- Hillenbrand, L. 2005, review article in “A Decade of Discovery: Planets Around Other Stars”, *STScI Symposium Series 19*, ed. M. Livio
- Hughes, A. M., Andrews, S. M., Espaillat, C., et al. 2009, *ApJ*, in press
- Hughes, A. M., Wilner, D. J., Calvet, N., D’Alessio, P., Claussen, M. J., & Hogerheijde, M. R. 2007, *ApJ*, 664, 536
- Ireland, M. J. & Kraus, A. L. 2008, *ApJ*, 678, L59
- Kennedy, G. M. & Kenyon, S. J. 2009, *ApJ*, in press
- Kenyon, S. J. & Hartmann, L. 1995, *ApJS*, 101, 117
- Kroupa, P. 2001, *MNRAS*, 322, 231
- Lada, C. J., Muench, A. A., Luhman, K. L. et al. 2006, *AJ*, 131, 1574
- Lawson, W. A., Crause, L. A., Mamajek, E. E., & Feigelson, E. D. 2002, *MNRAS*, 329, L29
- Lawson, W. A., Lyo, A.-R., & Muzerolle, J. 2004, *MNRAS*, 351, L39
- Loinard, L., Torres, R. M., Mioduszewski, A. J., & Rodríguez, L. F. 2008, *ApJ*, 675, L29
- Low, F. J., Smith, P. S., Werner, M., Chen, C., Krause, V., Jura, M., Hines, D. C. 2005, *ApJ*, 631, 1170
- Luhman, K. L. & Rieke, G. H. 1999, *ApJ*, 525, 440
- Luhman, K. L., Stauffer, J. R., Muench, A. A., Rieke, G. H., Lada, E. A., Bouvier, J., & Lada, C. J. 2003, *ApJ*, 593, 1093
- Luhman, K. L. & Steeghs, D. 2004, *ApJ*, 609, 917
- Mathis, J. S. 1990, *ARA&A*, 28, 37
- McCabe, C., Ghez, A. M., Prato, L., Duchêne, G., Fisher, R. S., & Telesco, C. 2006, *ApJ*, 636, 932
- Megeath, S. T., Hartmann, L., Luhman, K. L., & Fazio, G. G. 2005, *ApJ*, 634, L113
- Mitchell, G. F., Johnstone, D., Moriarity-Schieven, G., Fich, M., & Tothill, N. F. H. 2001, *ApJ*, 556, 215
- Moraux, E., Lawson, W. A., & Clarke, C. 2007, *A&A*, 473, 163
- Muzerolle, J., Calvet, N., Hartmann, L., D’Alessio, P. 2003, *ApJ*, 597, L149

- Padgett, D. L., Cieza, L., Stapelfeldt, K. R. et al. 2006, *ApJ*, 645, 1283
- Pollack, J. B., Hubickyj, O., Bodenheimer, P., Lissauer, J. J., Podolak, M., & Greenzweig, Y. 1996, *Icarus*, 124, 63
- Quillen, A. C., Blackman, E. G., Frank, A., & Varnière, P. 2004, *ApJ*, 612, L137
- Ratzka, T., Leinert, C., Henning, T., Bouwman, J., Dullemond, C. P., & Jaffe, W. 2007, *A&A*, 471, 173
- Rice, W. K. M., Armitage, P. J., Wood, K., & Lodato, G. 2006, *MNRAS*, 373, 1619
- Rice, W. K. M., Wood, K., Armitage, P. J., Whitney, B. A., & Bjorkman, J. E. 2003, *MNRAS*, 342, 79
- Sicilia-Aguilar, A., Hartmann, L., Briceño, C., Muzerolle, J., & Calvet, N. 2004, *AJ*, 128, 805
- Sicilia-Aguilar, A., Hartmann, L., Calvet, N. et al. 2006, *ApJ*, 638, 897
- Sicilia-Aguilar, A., Henning, T., Juhász, A., Bouwman, J., Garmire, G., & Garmire, A. 2008, *ApJ*, 687, 1145
- Siess, L., Dufour, E., & Forestini, M. 2000, *A&A*, 358, 593
- Skrutskie, M. F., Dutkevitch, D., Strom, S. E., Edwards, S., & Strom, K. M. 1990, *AJ*, 99, 1187
- Sterzik, M. E., Alcalá, J. M., Covino, E., & Petr, M. G. 1999, *A&A*, 346, L41
- Strom, K. M., Strom, S. E., Edwards, S., Cabrit, S., & Skrutskie, M. F. 1989, *AJ*, 97, 1451
- Uchida, K. I., Calvet, N., Hartmann, L. et al. 2004, *ApJS*, 154, 439
- Webb, R. A. et al. 1999, *ApJ*, 512, L63
- Weidenschilling, S. J. 1997, *Icarus*, 127, 290
- Wiling, B. A., Meyer, M. R., Greene, T. P., Mikhail, A., & Carlson, G. 2004, *AJ*, 127, 1131
- Winston, E., Megeath, S. T., Wolk, S. J. et al. 2007, *ApJ*, 669, 493
- Wood, K., Lada, C. J., Bjorkman, J. E., Kenyon, S. J., Whitney, B., & Wolff, M. J. 2002, *ApJ*, 567, 1183
- Zuckerman, B., Webb, R. A., Schwartz, M., & Becklin, E. E. 2001, *ApJ*, 549, L233

Table 1. Sample of young stellar clusters/associations

ID	t (Myr)	d (pc)	transition disk fraction
NGC 1333 ^a	$< 1^i$	320	1/66 (1.5 ^{+3.6} _{-1.2} %)
L 1688 ^b	$< 1^j$	140	1/74 (1.4 ^{+3.2} _{-1.1} %)
NGC 2068/2071 ^c	1-3 ^k	400	3/152 (2.0 ^{+1.9} _{-1.1} %)
IC 348 ^{d,e}	2-3 ^l	315	12/99 (12 ^{+4.2} _{-3.4} %)
OB1b ^f	4-6 ^k	400	1/14 (7.1 ⁺¹⁵ _{-5.7} %)
η Cha ^{g,h}	5-9 ⁿ	100	1/6 (17 ⁺²⁸ ₋₁₅ %)
OB1a/25 Ori ^f	7-10 ^m	330	1/6 (17 ⁺²⁸ ₋₁₅ %)

Note. — *Spitzer* data from: ^aGutermuth et al. (2008); ^bAllen et al. in preparation; ^cFlaherty & Muzerolle (2008); ^dLada et al. (2006); ^eMuench et al. (2007); ^fHernández et al. (2007); ^gMegeath et al. (2005); ^hGautier et al. (2008). Age estimates are taken from the literature: ⁱWilking et al. (2004); ^jLuhman et al. (2001); ^kFlaherty & Muzerolle (2008); ^lLuhman et al. (2003); ^mBriceño et al. (2005); ⁿLuhman & Steeghs (2004).

Table 2. Previously identified classical transition disks

ID	α (J2000)	δ (J2000)	SpT	A_V	$f_{5.8}$	W(H α)	accretor?
DM Tau ^a	04:33:48.73	+18:10:10.0	M1	0.5	...	-139	y
CoKu Tau/4 ^b	04:41:16.81	+28:40:00.0	M1	3.0	1.0	-1.8	n
GM Aur ^{a,c}	04:55:10.98	+30:21:59.4	K5	1.2	1.5	-97	y*
CVSO 224 ^d	05:25:46.74	+01:43:30.4	M3	0.2	1.3	-20.3	y*
TW Hya ^{c,e}	11:01:51.01	-34:42:17.0	K7	0.0	1.3	-220	y*
Hen 3-600A ^e	11:10:27.88	-37:31:52.0	M3	0.0	...	-22	y*
HD 98800 ^f	11:22:05.29	-24:46:39.8	K5	0.0	...	0	n*
CS Cha ^g	11:02:25.12	-77:33:36.0	K6	0.8	...	-20	y*

Note. — Based on *Spitzer* data from: ^aCalvet et al. 2005; ^bD’Alessio et al. 2005; ^cHartmann et al. 2005; ^dEspaillet et al. 2008b; ^eUchida et al. 2004; ^fFurlan et al. 2007; ^gEspaillet et al. 2007. Accretor status is based on the H α equivalent width, as explained in the text, except for those objects marked with *, where it is based on published high spectral resolution H α profiles.

Table 3. Classical transition disk candidates

ID	α (J2000)	δ (J2000)	SpT	A_V	$f_{5.8}$	W(H α)	accretor?
DoAr 21 ^a	16:26:03.01	-24:23:37.9	K0	6.3	1.5	-0.6	n
LAL 31	03:29:29.26	+31:18:34.9	K5	4.5	1.1	-8.4	y
LRL 21 ^b	03:44:56.15	32:09:15.5	K0	5.4	1.5	-4.7	y*
LRL 31 ^b	03:44:18.16	32:04:57.0	G1	11.9	1.6	-11	y*
LRL 67 ^b	03:43:44.62	32:08:17.9	M0.75	2.4	1.2	-35	y*
LRL 72 ^b	03:44:22.57	32:01:53.7	M2.5	2.5 (3.5)	1.0	-3.5	n
LRL 97 ^b	03:44:25.56	32:06:17.0	M2.25	4.6 (6.0)	1.4	-3.0	n
LRL 133 ^b	03:44:41.74	32:12:02.4	M5	3.9	1.4
LRL 190 ^b	03:44:29.21	32:01:15.8	M3.75	7.1	1.3	-5.0	n
LRL 237 ^b	03:44:23.57	32:09:34.0	M5	1.7	1.4	-6.0	n
LRL 297 ^b	03:44:33.21	32:12:57.5	M4.5	7.8 (8.4)	1.4
LRL 301 ^b	03:44:22.70	32:01:42.4	M4.75	6.2	1.3	-40	y
LRL 316 ^b	03:44:57.73	32:07:41.9	M6.5	1.2	1.0	-4.0	n
LRL 1679 ^c	03:44:52.06	31:58:25.2	M3.5	5.7	1.5
FM 177 ^d	05:45:41.95	-00:12:05.3	K4	1.8	0.9	-1.2	n*
FM 281 ^d	05:45:53.11	-00:13:24.9	M1	1.1	1.1	-18.1	y*
FM 856 ^d	05:46:44.85	+00:16:59.7	M1	4.2	1.4	-14.0	y*
CVSO 95 ^e	05:31:39.00	-01:27:46.0	M5	0.0	1.1	-8.9	n
CVSO 224 ^f	05:25:46.74	+01:43:30.4	M3	0.2	1.3	-20.3	y*
RECX 5 ^g	08:42:27.10	-78:57:47.9	M4	0.0	1.2	-35.0	y*

Note. — Spectral types and H α measurements from: ^aBouvier & Appenzeller (1992); ^bLuhman et al. (2003); ^cMuench et al. (2007); ^dFlaherty & Muzerolle (2008); ^eBriceño et al. (2005); ^fBriceño et al. (2007); ^gLawson et al. (2004). If the extinction was adjusted for a better SED fit (see text), the original value from the literature is listed in parentheses. Accretor status is marked as in Table 2.

Table 4. Warm excess transition candidates

ID	α (J2000)	δ (J2000)	SpT	A_V	$f_{5.8}$	W(H α)	accretor?
LRL 58 ^a	03:44:38.55	32:08:00.7	M1.25	3.7	1.9	-9.0	n
LRL 110 ^a	03:44:37.40	32:12:24.3	M2	4.6 (5.3)	1.8	-22.	y
LRL 194 ^a	03:44:27.25	32:10:37.3	M4.75	3.1	2.2	-100.	y
FM 326 ^b	05:45:56.31	00:07:08.6	K7	1.6	2.3	-6.2	y*
FM 515 ^b	05:46:11.86	00:32:25.9	K2	1.3	3.9	-3.8	y*
FM 618 ^b	05:46:22.44	-00:08:52.6	K1	2.6	2.5	-32	y*

Note. — Spectral types and H α measurements from: ^aLuhman et al. (2003); ^bFlaherty & Muzerolle (2008). If the extinction was adjusted for a better SED fit (see text), the original value from the literature is listed in parentheses. Accretor status is marked as in Table 2.

Table 5. Weak excess transition candidates

ID	α (J2000)	δ (J2000)	SpT	A_V	$f_{5.8}$	W(H α)	accretor?
GY 326 ^a	16:27:42.70	-24:38:50.6	M4	10.0 (11.4)	1.2
LRL 6 ^b	03:44:36.94	32:06:45.4	G3	3.2 (3.9)	1.5	0.7	n*
LRL 30 ^c	03:44:19.13	32:09:31.4	F0	0.3 (1.9)	1.0
LRL 68 ^c	03:44:28.51	31:59:54.1	M3.5	1.8 (2.9)	1.6	-5.1	n
LRL 76 ^c	03:44:39.81	32:18:04.2	M3.75	3.1	1.6	-14	n
LRL 135 ^c	03:44:39.19	32 20:09.0	M4.5	1.1 (2.0)	1.6	-20	y
LRL 176 ^c	03:45:04.63	32 15:01.1	M4.25	4.1	1.0
LRL 182 ^c	03:44:18.20	32:09:59.3	M4.25	2.5 (3.1)	1.4	-6.0	n
LRL 213 ^c	03:44:21.27	32:12:37.3	M4.75	1.4 (2.1)	1.7	-6.0	n
LRL 214 ^c	03:44:07.51	32:04:08.9	M4.75	1.1 (2.1)	1.5	-7.0	n
LRL 229 ^c	03:44:57.86	32:04:01.8	M5.25	1.2	1.2	-4.5	n
LRL 241 ^c	03:44:59.84	32:13:32.2	M4.5	2.8 (3.2)	1.5	-80	y
FM 458 ^d	05:46:07.89	-00:11:56.9	K3	4.0	1.2	-3.2	y*
FM 543 ^d	05:46:14.48	00:20:24.4	M4	1.8	1.4	-3.6	n*
FM 998 ^d	05:46:58.13	00:05:38.2	M0	3.7	1.2	-2.0	y*
FM 1056	05:47:03.32	00:23:23.5	M3	7.5	1.7
OB1b-337 ^e	05:29:35.44	-01:39:38.9	K7	0.0	0.93	-1.3	n
CVSO 103/OB1b-1810 ^f	05:32:06.41	-01:26:43.5	M2	0.0	1.5	-20	y
OB1b-2266 ^e	05:32:43.71	-01:58:10.9	M3.5	0.0	1.4	-3.7	n
OB1a-905 ^e	05:24:58.85	+01:25:18.3	M5	0.0	1.3	-15	n
CVSO 217/OB1a-1121 ^f	05:25:34.40	+01:52:19.7	M1	0.0	0.98	-2.1	n
OB1a-1695 ^e	05:27:02.95	+01:39:00.8	M5	0.0	1.0	-6.7	n
RECX 9 ^g	08:44:16.37	-78:59:08.0	M4.5	0.0	1.3	-10.0	y*
ECHA J0841.5-7853 ^g	08:41:30.30	-78:53:06.4	M4.75	0.0	1.4	-12.0	n*
ECHA J0844.2-7833 ^h	08:44:09.14	-78:33:45.7	M5.75	0.0	1.7

Note. — Spectral types and H α measurements from: ^aLuhman et al. (2001); ^bDahm (2008); ^cLuhman et al. (2003); ^dFlaherty & Muzerolle (2008); ^eBriceño et al. in preparation; ^fBriceño et al. (2007); ^gLawson et al. (2002); ^hLuhman & Steeghs (2004). If the extinction was adjusted for a better SED fit (see text), the original value from the literature is listed in parentheses. Accretor status is marked as in Table 2.

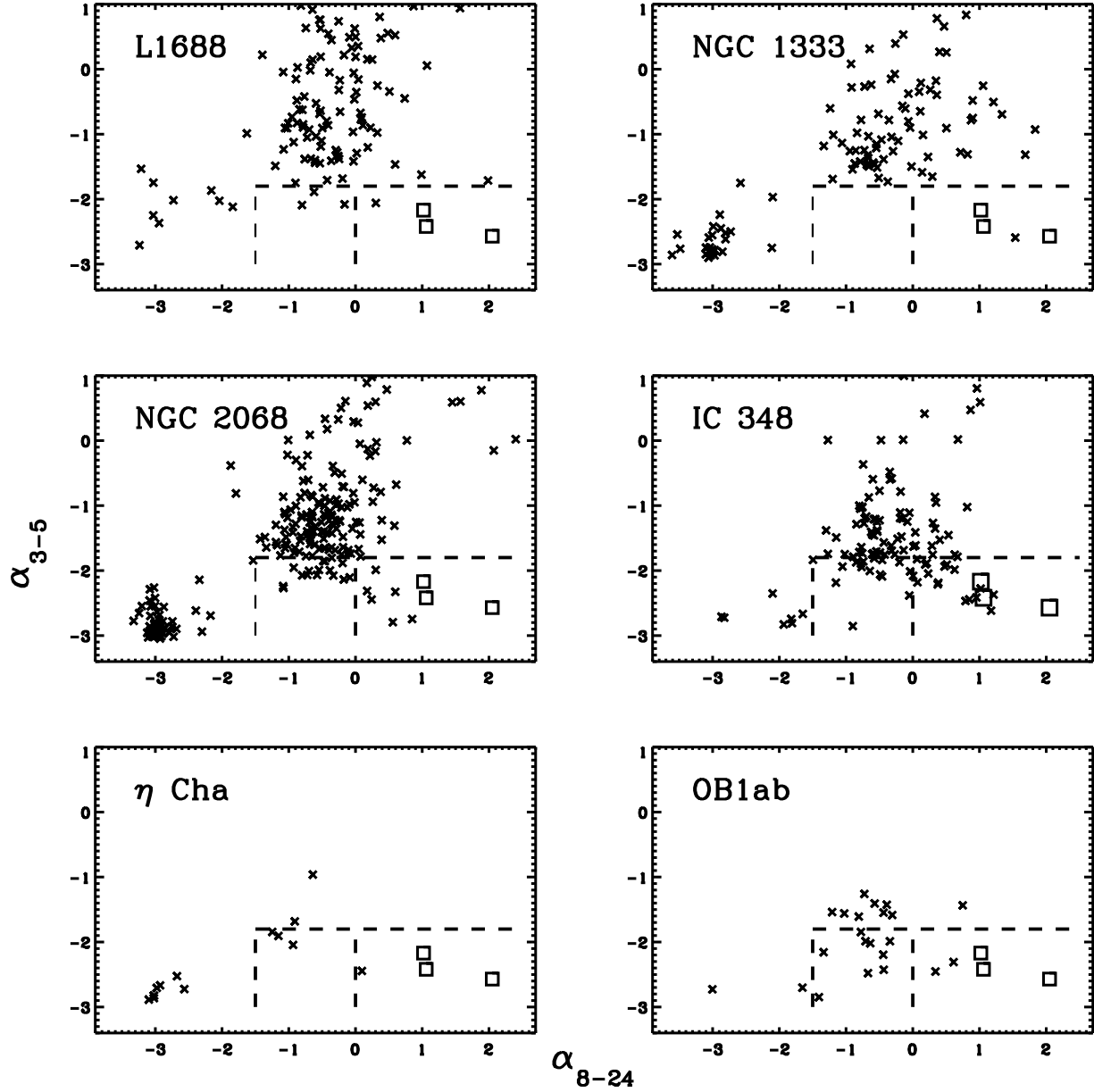


Fig. 1.— IRAC-MIPS spectral slope comparison. *Crosses*: all objects detected at 3.6, 4.5, 5.8, 8, and 24 μm in L 1688, NGC 1333, and NGC 2068 (some very red objects are off the top edge of the plots), and confirmed members only for IC 348, the η Cha association and the Orion OB1a and b associations. *Squares*: the known transition objects GM Aur, TW Hya, and CoKu Tau/4 (from left to right). Dashed lines mark the adopted region for selecting transition disk candidates (see text).

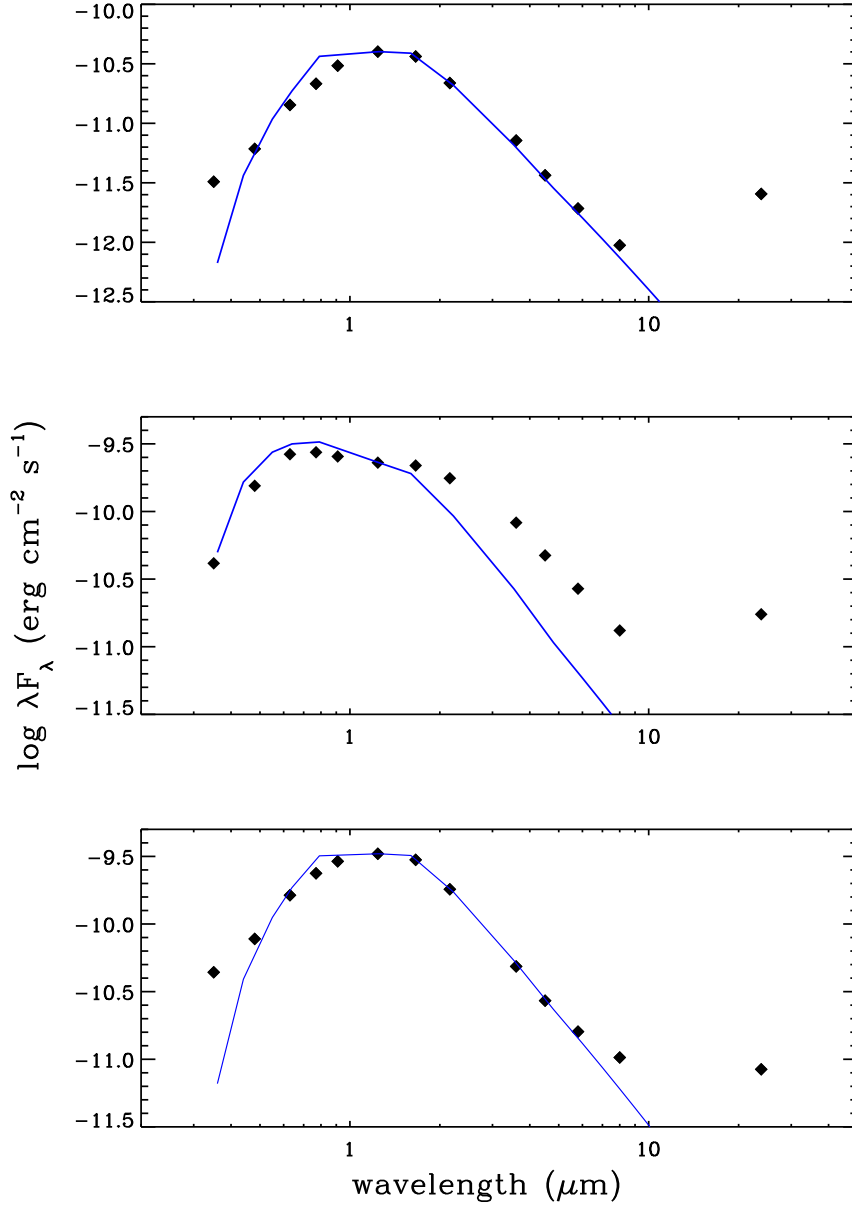


Fig. 2.— SEDs of two inner disk hole candidates identified from the spectral slope locus shown in Figure 1 (top two panels), plus one object satisfying only the short wavelength criterion (bottom panel). Diamonds are observed fluxes dereddened using the known A_V of each star and the Mathis (1990) and Flaherty et al. (2007) reddening law. Optical and infrared photometry and stellar properties are reported in Flaherty & Muzerolle (2008). Solid blue lines are empirical photospheres constructed from the main sequence star colors from Kenyon & Hartmann (1995), normalized to the observed J -band flux.

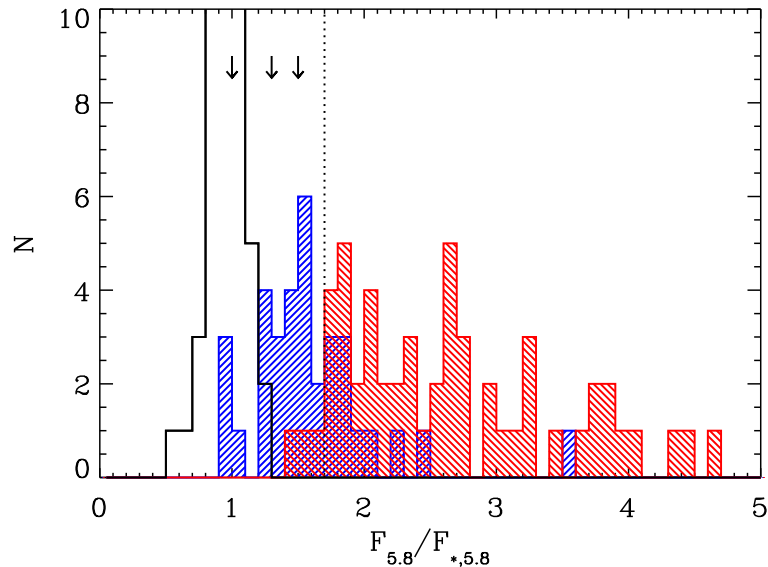


Fig. 3.— The distribution of observed to photospheric flux ratios at $5.8 \mu\text{m}$ for IC 348 members. The open histogram shows flux ratios for all objects whose $3\text{-}5 \mu\text{m}$ spectral slopes and lack of $24 \mu\text{m}$ detections indicate no substantial circumstellar material (the peak is off the plot at $N = 56$). The hatched histograms represent flux ratios for sources with disks and detections out to $24 \mu\text{m}$: positive-slope hatching represents objects with $\alpha_{3-5} < -1.8$, negative-slope hatching represents all other disks. There are 8 objects with flux ratios from 5-15 not shown. The arrows indicate the flux ratios of three known classical transition disks (from left to right: CoKu Tau/4, TW Hya, GM Aur). The dotted line indicates the cut-off value for our final transition disk selection.

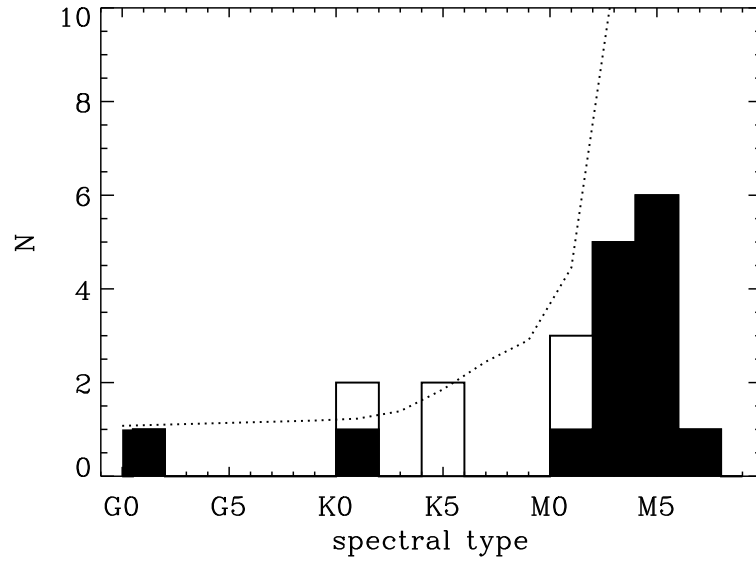


Fig. 4.— Distribution of spectral types for the classical transition objects identified in this paper. The solid histogram shows the distribution for the transition disks in the four oldest regions (IC 348, η Cha, and Orion OB1ab). The stellar mass function from Kroupa (2001), arbitrarily scaled to G0, is shown with the dotted line.

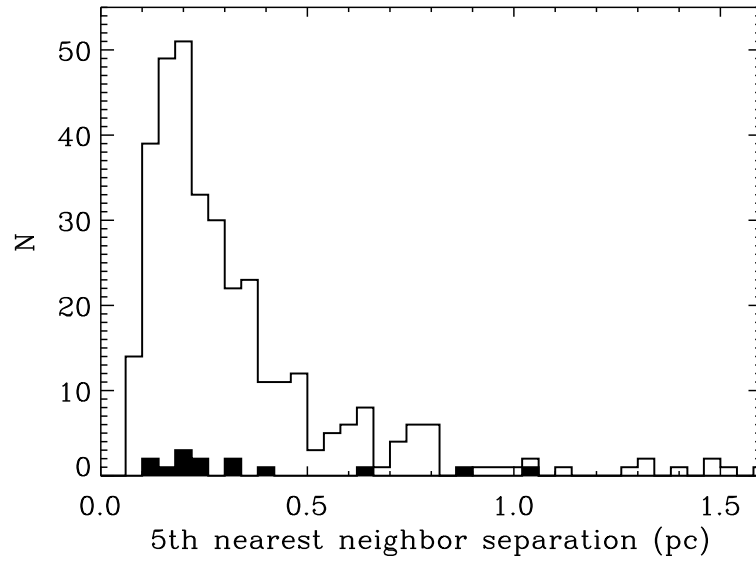


Fig. 5.— Fifth-nearest neighbor distribution for the classical transition disks (solid histogram) and all other disks detected out to $24 \mu\text{m}$ (open histogram) for the combined sample in L1688, NGC 1333, NGC 2068/2071, and IC 348.

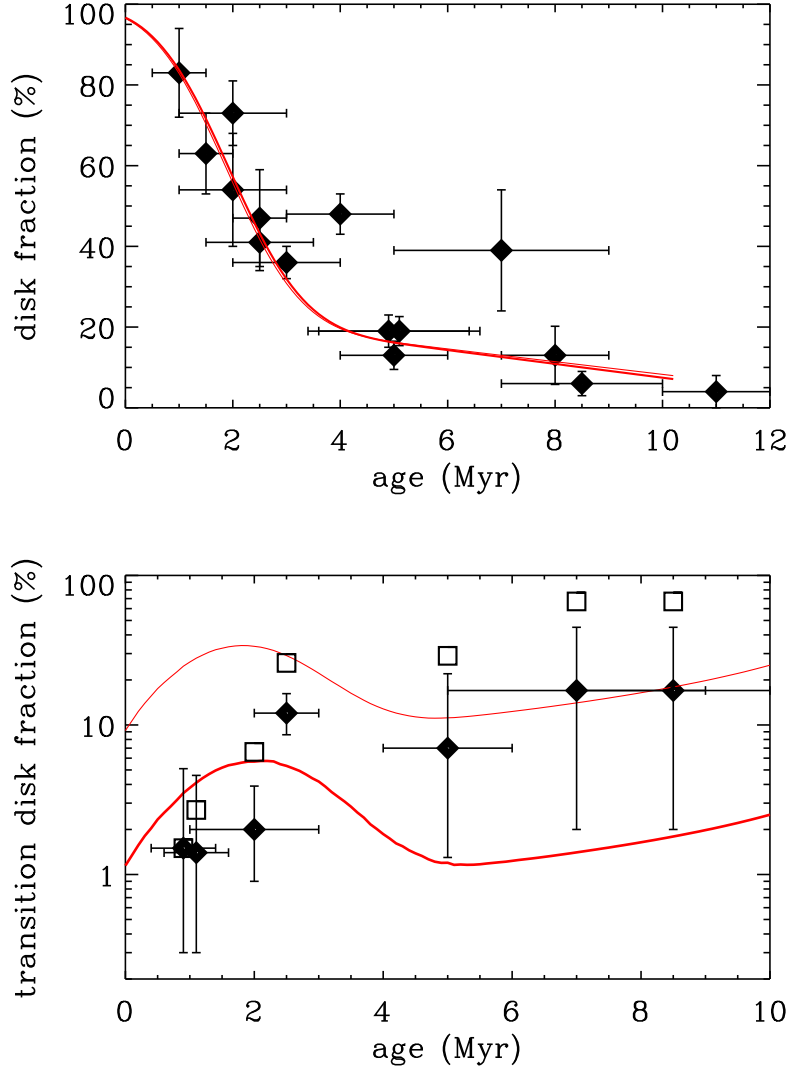


Fig. 6.— *Top panel:* The fraction of all members of a given young cluster or association that exhibit infrared excess indicative of protoplanetary disks (data from Gutermuth et al. 2008; Furlan et al. 2006; Flaherty & Muzerolle 2008; Lada et al. 2006; Balog et al. 2006; Gutermuth et al. 2004; Sicilia-Aguilar et al. 2006; Hernández et al. 2007ab; Carpenter et al. 2006; Dahm & Hillenbrand 2007; Megeath et al. 2005; Low et al. 2006). The points near $t = 5$ Myr, $f_d = 20\%$ (representing Upper Sco and NGC 2362) have been shifted slightly in age for clarity. The solid line shows our adopted two-component parametric model for disk dissipation with two different transition timescales: 0.1 Myr (thick) and 1 Myr (thin). *Bottom panel:* The percentage of protoplanetary disks in a given region that exhibit SEDs consistent with classical transition disks (diamonds). The open squares represent the percentages including the warm and weak excess classes. The solid lines show the predicted values from the dissipation model for the 0.1 and 1 Myr transition timescales.

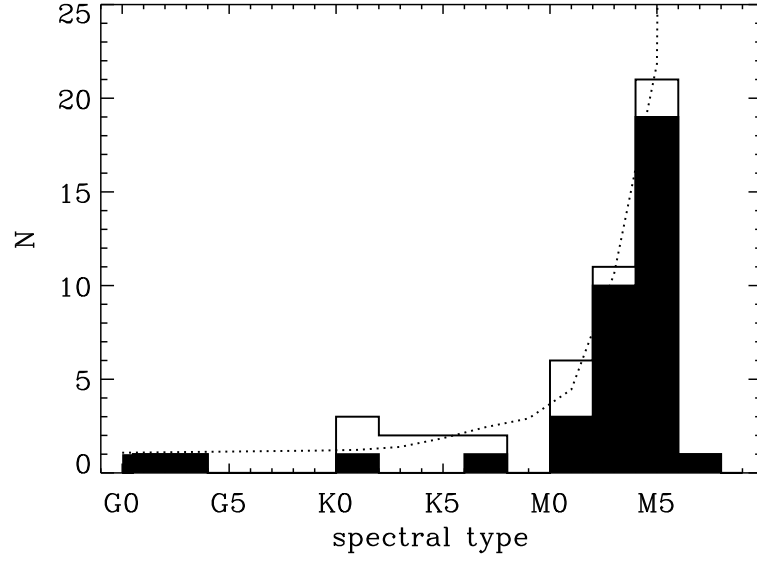


Fig. 7.— Same as in Figure 4, with the warm and weak excess transition objects added in.